Emission characteristics of size distribution, chemical composition and light absorption of particles from field-scale crop residue burning in Northeast China

Qinglu Wang [a,g,1], Lili Wang [a,g,*,1], Xingru Li [c], Jinyuan Xin [a,g], Zirui Liu [a], Yang Sun [a,g], Jingda Liu [h], Yanjun Zhang [j], Wei Du [j], Xin Jin [a,g], Tianran Zhang [i], Shuiqiao Liu [c], Quan Liu [e], Jie Chen [f], Miaomiao Cheng [d,**], Yuesi Wang [a,b,g]

[a] State Key Laboratory of Atmospheric Boundary Layer Physics and Atmospheric Chemistry, Institute of Atmospheric Physics, Chinese Academy of Sciences, Beijing 100029, China
[b] Center for Excellence in Regional Atmospheric Environment, Institute of Urban Environment, Chinese Academy of Sciences, Xiamen 361021, China
[c] Capital Normal University, Beijing 100037, China
[d] State Key Laboratory of Environmental Criteria and Risk Assessment, Chinese Research Academy of Environmental Sciences, Beijing 100012, China
[e] Beijing Weather Modification Office, Beijing Meteorological Bureau, Beijing 100089, China
[f] National Satellite Meteorological Centre of China Meteorological Administration, Beijing 100049, China
[g] College of Earth Sciences, University of Chinese Academy of Sciences, Beijing 100049, China
[h] College of Atmospheric Physics, Nanjing University of Information Science & Technology, Nanjing 210044, China
[i] King's College London, Earth and Environmental Dynamics Research Group, Department of Geography, Strand, London WC2R 2LS, UK
[j] Institute for Atmospheric and Earth System Research/Physics, Faculty of Science, University of Helsinki, Helsinki, 00014, Finland

HIGHLIGHTS

- The characteristics of physical, chemical and optical of particles from crop residue open burning were investigated.
- The higher number concentrations of particles (250 to 3200 nm) were emitted during flaming than smoldering phase.
- Organic carbon, element carbon, Cl⁻ and K^+ in $PM_{2.5}$ from fresh smoke plume were abundant components.
- The contribution of BrC to total aerosol light absorption increases as wavelength and EC/OC decreases and AAE increases.
- Combustion condition affected the optical properties of carbonaceous aerosols and absorption contribution of BrC.

GRAPHICAL ABSTRACT
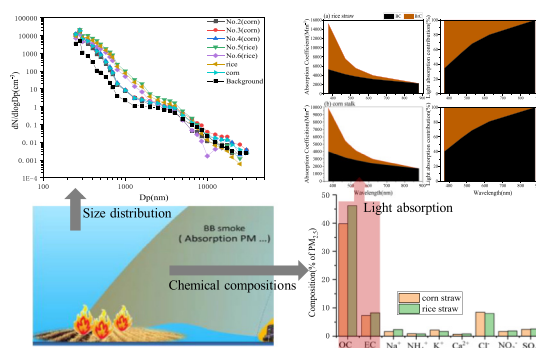
ARTICLE INFO

ABSTRACT

Crop residue burning in China increased significantly in the last decade, especially it took up a majority in Northeast China, which plays an important role of severe haze pollution. Hence, two main types of crop residues (corn and rice straw) were chosen to characterize the particle number concentration, chemical components of fine particulate matter and optical properties of carbonaceous aerosols by a suite of fast-response online portable instruments, together with offline sampling and analysis, during the field-based combustion experiments in Northeast

---

 * Correspondence to: L. Wang, State Key Laboratory of Atmospheric Boundary Layer Physics and Atmospheric Chemistry, Institute of Atmospheric Physics, Chinese Academy of Sciences, Beijing 100029, China.
 ** Corresponding author.
   E-mail addresses: wll@mail.iap.ac.cn (L. Wang), chengmm@craes.org.cn (M. Cheng).
 [1] These authors contributed equally to this work.

China. For the range of 250 and 2500 nm, more particles were emitted from rice straw burning than those from corn straw burning, and the time-averaged number concentration of particles during the flaming process was approximately 2 times higher than that during the smoldering process for these two straws. Organic carbon (OC), elemental carbon (EC) and water-soluble ions were the most abundant components and accounted for $42.5 \pm 7.5\%$, $7.7 \pm 1.7\%$ and $18.0 \pm 3.4\%$ of the $PM_{2.5}$, respectively. Furthermore, rice straw burning emitted higher OC and lower Cl^- and K^+ than those from corn straw burning. The average absorption Ångström exponent (AAE) of carbonaceous aerosols was 2.1 ± 0.3, while the AAE of brown carbon (BrC) was 4.7 ± 0.4 during the whole burning process. On average, BrC contributed to 63% and 20% of the total light absorption at 375 nm and 625 nm, respectively. Parameterization of BrC absorption revealed that the fraction of absorption from BrC has a reasonably good correlation with EC/OC (-0.84) and AAE (0.94) at 375 nm. Generally, combustion conditions can affect the optical properties of carbonaceous aerosols, and a negative correlation (-0.77) was observed between the AAE and modified combustion efficiency; in addition, the percentage of absorption due to BrC were lower at the flaming phase.

1. Introduction

Biomass burning (e.g. grassland or forest fires and agricultural waste burning) emitted abundant gaseous and particulate pollutants into the atmosphere (Koppmann et al., 2005; Reid et al., 2005a; Reid et al., 2005b), which has been recognized as a major sources of aerosols. The global and regional radiation budget can be influenced by aerosols from biomass burning through direct and indirect radiative forcing and cloud processes (Penner et al., 1992); however, the climate effect assessment has the great uncertainty due to the need to resolve the balance between the positive radiative forcing by black carbon (BC) and brown carbon (BrC), and the negative radiative forcing by OC and inorganics (J. Chen et al., 2017; IPCC, 2013). In addition, biomass burning have significant impacts on regional and local air quality and public health (J. Chen et al., 2017; X. Ding et al., 2016; Huang et al., 2016; Islam et al., 2015; Kim et al., 2013; Wang et al., 2017).

As the world's major agricultural country, China's annual agricultural residues account for 17.3% of the global agricultural crops, ranking first in the world (Yuyun et al., 2010). The amount of straw burning was 160 million tons annually, accounting for >50% of the total biomass combustion amount (Yan et al., 2006). With the improvement of rural people's living standards and infrastructure, crop residues were increasingly burned directly in the cropland after harvest. Crop residues burning in China increased significantly in the last decades (Zhuang et al., 2018). Zhang et al. (2016) estimated that the annual average $PM_{2.5}$ Chinese straw burning emission from 1997 to 2013 was 1036 Gigagrams (Gg) based on crop yields and burning detection by satellites. Biomass burning has a significant impact on air quality over the Pearl River Delta, the Yangtze River Delta, the Beijing-Tianjin-Hebei region and Northeast China and aggravates the levels of regional and urban haze pollution during the harvest season (J. Chen et al., 2017; W. Chen et al., 2017; Cheng et al., 2013; Li et al., 2014; Wang et al., 2013; Wang et al., 2015).

In particular, agricultural open burning has become severe in Northeast China (Fig. 1a). The burned area of crops in Mar and Apr increased year by year from 2028 km² in 2013 to 16051 km² in 2017, and it also changed annually in Oct and Nov, with the highest value observed in 2014 and lowest value observed in 2016 (Ke et al., 2019); in addition, crop residue burning spots in Northeast China account for a major proportion in the total number of that in China (Zhuang et al., 2018). In recent years, Northeast China has become the new heavily polluted area in China due to its persistent, heavy and widespread haze pollution. Some studies illustrated that agricultural straw burning was one of the main sources for heavy pollution during the crop harvest season (Cao et al., 2017; W. Chen et al., 2017; Mehmood et al., 2017; Zhang et al., 2016). The smoke plumes emitted from straw burning become mixed with the urban pollution emissions, which results in the explosive growth of secondary fine particulates over a short time under stagnant weather conditions (A.J. Ding et al., 2016; Huang et al., 2016; Wang et al., 2015). Therefore, studies on the characteristics of fresh aerosol which emitted from straw burning smoke in Northeast China are particularly urgent for exploring the causes and quantitative contributions to air pollution.

Many studies on the characteristics of aerosols released from straw burning were carried out primarily based on simulated agricultural fires in a combustion chamber in the laboratory; however, only a few experiments were conducted in the fields. From laboratory combustion experiments, Chakrabarty et al. (2010) observed that the particle size distributions are cabined with a single diameter peak at 70 nm for wood and grass, and Hays et al. (2005) reported the mode in their size distributions were about 100 nm for wheat straw burning in an enclosure. LeCanut et al. (1996) obtained two mass modes in range 0.2–0.3 μm and above 2 μm, when particle size distribution was measured by using a laser optical particle counter in airborne study during a savanna fire in Southern Africa. Alonso et al. (2012) revealed that the number of particles in sizes between 0.10 and 0.14 μm were nearly 20 times higher than background during the wildfires that occurred in Spain. $PM_{2.5}$ source profiles on crop burning have been obtained in many studies (Li et al., 2007; Ni et al., 2017; Sun et al., 2019b). Ni et al. (2017) and Sun et al. (2019b) obtained the chemical profiles of the carbonaceous fraction, water–soluble ions and elements for several crop straws burned in a laboratory combustion chamber. BrC from biomass burning has been investigated directly through a series of laboratory experiments, and it contributed to 41–85% of the total light absorption at 370 nm (Tian et al., 2019) and 92% and 58% of the total absorption at 405 nm and 532 nm, respectively (Pokhrel et al., 2017).

Laboratory simulated experiments can reflect the characteristics of straw burning to a certain extent; however, meteorological conditions and the underlying soil surface in the field environment cannot be simulated. In addition, we still cannot accurately evaluate radiative forcing, regional environment and climate change because of the lack of BC and BrC absorption characteristics from fresh straw combustion smoke in the field. In this study, typical biomass materials, e.g., corn and rice straw, were burnt in an open field experiment in Northeast China. The concentrations of CO and CO_2, the evolution of the particle size distribution, and the absorption values of BC and BrC were measured by fast-response online portable instruments, and the components of $PM_{2.5}$ were all obtained via sampling and offline analysis. A new portable multi-wavelength aethalometer was first applied to calculate the light absorption coefficient of particles (BC and BrC) emitted from fresh field-based residual smoke plume. Generally, this paper attempts to capture the transient and integrated characteristics of the particle size distribution, chemical components, and optical absorption of particles, which are important parameters as they affect air quality, climate modelling and health effects. Our findings will help to quantify the contribution of open agricultural burning to air pollution and establish the suitable strategies to mitigate haze pollution.
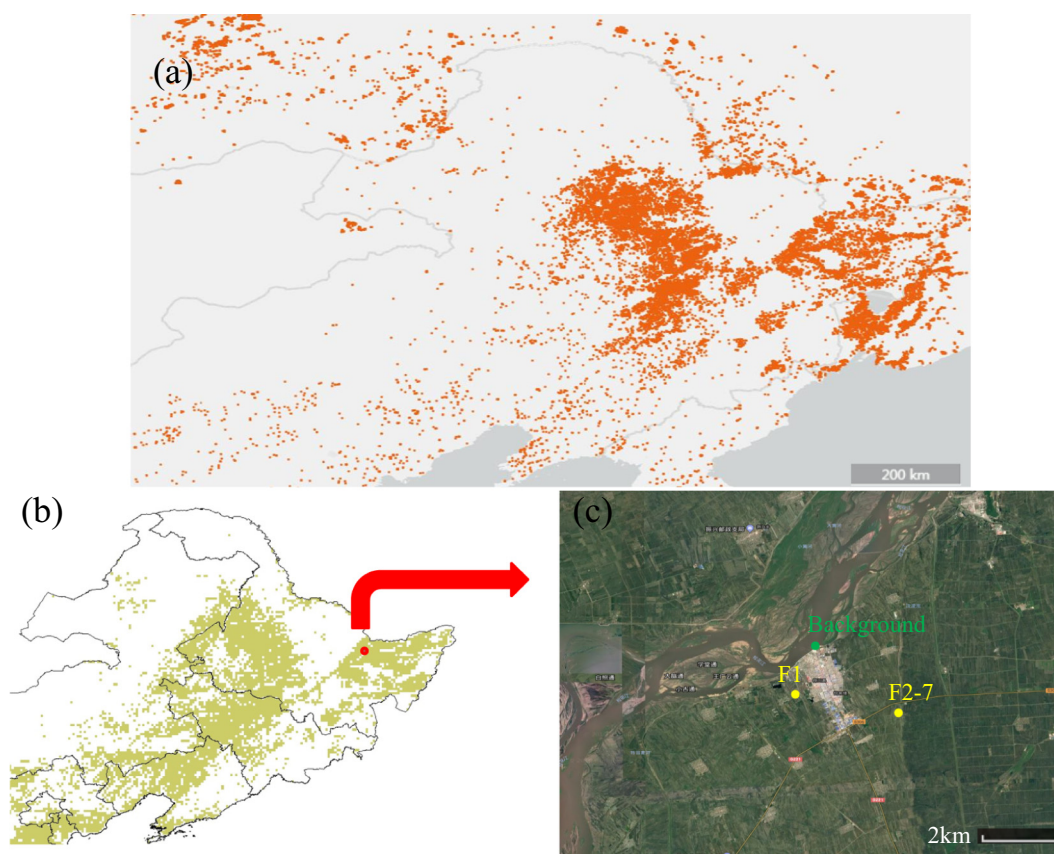
Fig. 1. (a) Map of fire points in Northeast China during April 2017 from Terra and Aqua MODIS C6 products (https://firms.modaps.eosdis.nasa.gov/map/). (b) Farmland distribution map for Northeast China. (c) Location of the sampling site in this study (Huachan County, Jiamusi city of Heilongjiang Province). The yellow and green points indicate the sampling and background sites, respectively. (For interpretation of the references to color in this figure legend, the reader is referred to the web version of this article.)

2. Instruments and methods

2.1. Experiment site and methods

The experiments were conducted in a rural area in Huachuan County (46°37′N–47°14′N, 130°16′E–131°34′E) from April 24 to April 25, 2018. Huachuan County is located in the city of Jiamusi of Heilongjiang Province, China (Fig. 1). Corn straw and rice straw, two main crops in Northeast China, were chosen to be burned in a manner similar to normal burning in the fields by local farmers. Each test lasted 18–48 min and included flaming and smoldering. Fire No. 1 and 7 occurred in an open area of the field. Fire Nos. 2–6 were spread in two windrows. The width and length of each windrow were 1 m and 5–10 m, respectively. The space between the two windrows was approximately 1 m. More detailed information about each test is summarized in Table 1.

The temperature (T) and relative humidity (RH) during the experiments ranged from 16 to 26 °C and from 20 to 55%, respectively. The

wind direction (WD) was always southwest with wind speed range from 1.4 to 4.4 m s^{-1}. The headfire ignition technique was applied to simulate the common open burning practice in the field, and smoke plumes were collected at the back of the smoke. Because smoke was difficult to collect under the conditions of weak winds or strong winds, a new sampling system with a high-flow air pump was designed, which was settled at the end of an aluminum pipe (length of 8 m and diameter of 16 cm). To reduce the wall effect as much as possible and reflect the actual situation of the smoke, the inlets of the instruments (the diameter of all instruments is <2 cm) were placed in the middle of the pipe and approximately 1 m away from the suction pump. Smoke was collected within a range of 5–10 m from the fire source by the pipe with two brackets. The smoke plume temperature dropped to approximately 30 °C, and the smoke also lacked sufficient physical and chemical reactions. This method of collection preserved particulate matter characteristics from open burning sources and satisfied the requirements of the instrument range. The quartz filters were kept in a portable refrigerator after sampling. We also analyzed the characteristics of the aerosols of

Table 1
Detail of the fires as measured in Northeast China during the April 2018 field campaign.

Fire no.	Fuel	Date	Burning time	Fire duration	Fire type	Observation factors
1	Rice straw	4–24	15:11–15:54	43 min	Spreading	CO, CO$_2$, BC, BrC, PM$_{2.5}$
2	Corn straw	4–25	13:51–14:09	18 min	Spreading	CO, CO$_2$, BC, BrC, PM$_{2.5}$, PNC[a]
3	Corn straw	4–25	15:08–15:46	38 min	Spreading	CO, CO$_2$, BC, BrC, PM$_{2.5}$, PNC
4	Corn straw	4–25	16:14–16:41	27 min	Spreading	CO, CO$_2$, BC, BrC, PM$_{2.5}$, PNC
5	Rice straw	4–25	17:02–17:32	30 min	Spreading	CO, CO$_2$, BC, BrC, PM$_{2.5}$, PNC
6	Rice straw	4–25	17:47–18:08	21 min	Spreading	CO, CO$_2$, BC, BrC, PM$_{2.5}$, PNC
7	Corn straw	4–25	18:23–18:54	31 min	Spreading	CO, CO$_2$, BC, BrC, PM$_{2.5}$

[a] PNC denotes particle number concentration.

the ambient background to compare with the smoke from biomass burning.

2.2. Instruments and analysis of the aerosol chemical composition

A portable $PM_{2.5}$ filter sampler (Model Omni, BGI Inc., USA) was used with a flow rate of 5 L min^{-1} in the experiments. This instrument is widely used in the field where the environment is harsh and electricity

is not conveniently provided (J. Chen et al., 2017; Zhang et al., 2015). Each aerosol sample was collected during every completed experiment. The ambient background aerosols were sampled after burning experiment (Fig. 1c). The sampler consisted of a 47 mm quartz-fiber filter that collected samples for OC, EC and water-soluble ion analyses. Prior to sampling, the quartz filters were baked at 450 °C for 2 h to reduce the blank carbon levels. Before and after sampling, the filters were conditioned for 48 h at approximately 50% RH and 25 °C in an air-
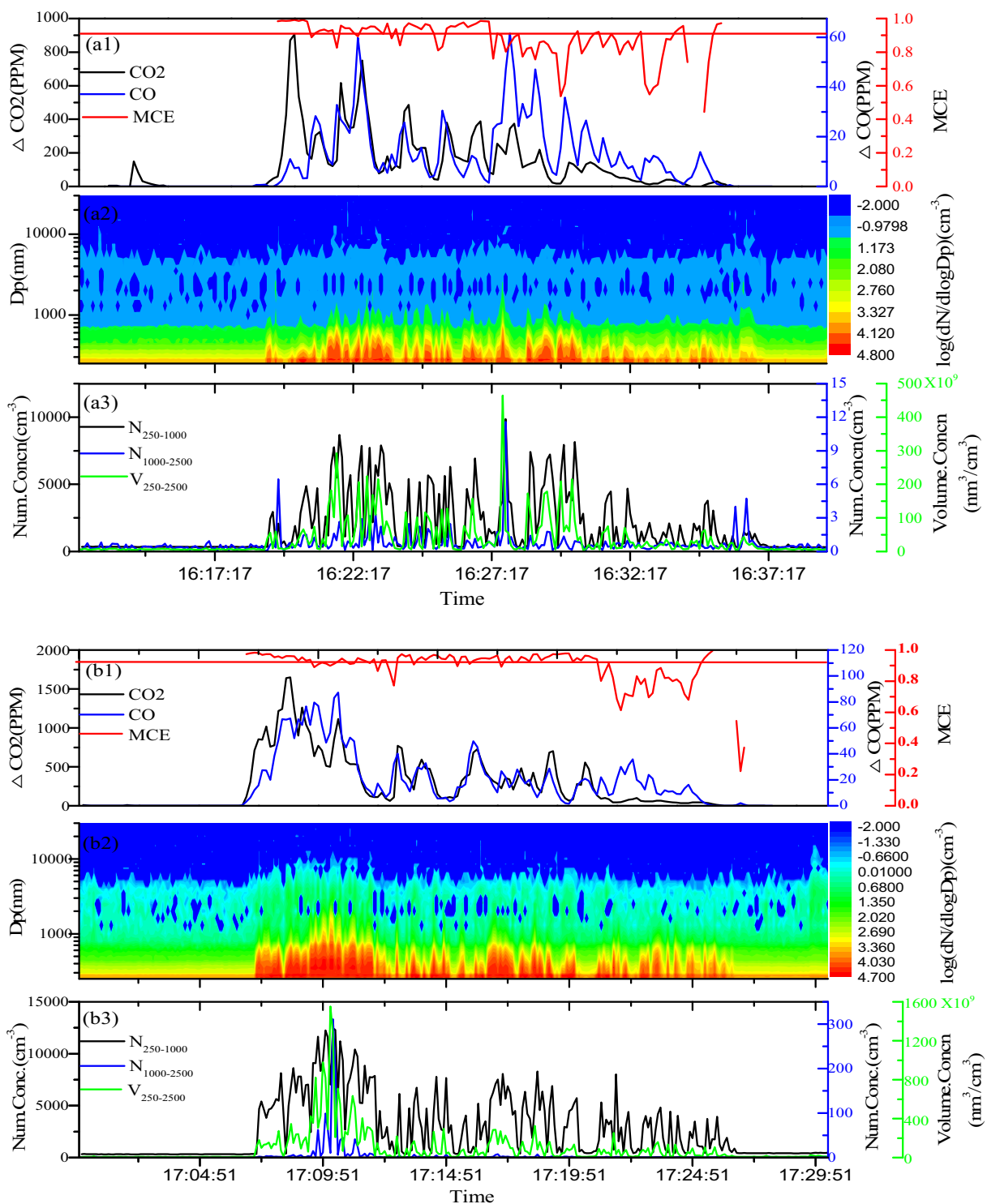

Fig. 2. Time series of the excess CO_2 and CO mixing ratio, MCE, particle size distribution, and particle number and volume concentrations for (a) corn straw (Fire No. 4) and (b) rice straw (Fire No. 5). $N_{250-1000}$ and $N_{1000-2500}$ represents the total particles from 250 to 1000 nm, and from 1000 to 2500 nm, respectively. $V_{250-2500}$ represents the total volume concentration from 250 to 2500 nm.

Table 2
Average concentration, median value, maximum value and minimum value of the fine particles ($N_{250-1000}$) and coarse particles ($N_{1000-2500}$) from crop burning.

Fuel	$N_{250-1000}$[a] (cm^{-3})				$N_{1000-2500}$[b] (cm^{-3})			
	Mean ± SD	Median	Max	Min	Mean ± SD	Median	Max	Min
Rice straw	3525.3 ± 46.7	2892.0	13,334.6	440.9	9.1 ± 4.8	0.9	440.9	0.05
Corn straw	2139.0 ± 398.1	1314.8	10,843.0	319.1	0.8 ± 0.1	0.5	13.9	0.05
Background	338.3 ± 117.4	252.5	708.3	145.2	0.3 ± 0.1	0.2	0.9	0.1

[a] $N_{250-1000}$ denotes total particles from 250 to 1000 nm.
[b] $N_{1000-2500}$ denotes total particles from 1000 to 2500 nm.

conditioned room and weighed on a microbalance with a resolution of 10 µg. The analysis of the water-soluble anions (F^-, NO_2^{2-}, NO_3^-, SO_4^{2-}, and Cl^-) was carried out using an ion chromatography system (ICS-1100, Dionex, USA); the water-soluble cations (Na^+, K^+, Ca^{2+}, Mg^{2+}, and NH_4^+) were analyzed with an ICS-80 (Dionex, USA). The concentrations of EC and OC were measured using a thermal carbon aerosol analyzer (DRI Model 2001A, Desert Research Institute, USA) (Li et al., 2012).

The aerosol particle number concentration was measured using a Grimm optical particle counter model OPC 11-C (Grimm Aerosol Technik GmbH & Co. KG, Ainring, Germany). This instrument has 31 size channels in the range of 250–32000 nm and can measure a particle concentration range from 0 to $10^6 L^{-1}$. The flow rate and time resolution were 1.2 L min^{-1} and 6 s, respectively. The number concentration measured by the OPC had a strong correlation with that by differential mobility analyzers (DMAs) (Burkart et al., 2010).

The CO and CO_2 levels were measured by a GT-2000, which was manufactured by the Korno Company. An electrochemical sensor and nondispersive infrared (NDIR) sensor were applied to analyze CO and

CO_2, respectively. The CO and CO_2 sensor measurement ranges are 0–100 ppm and 0–2000 ppm, respectively, and the resolution is 0.01 ppm and 1 ppm, respectively. The temporal resolution was set to 10 s.

A newly developed multi-wavelength aethalometer (model MA200, Aethlabs, United States) instrument, which has five wavelengths ($\lambda = $ 375, 470, 528, 625, and 880 nm), was used to observed the light absorption coefficients of the carbon aerosols with the 100 mL min^{-1} flow rate and 10 s time resolution. The model MA200 aethalometer analyzes samples on two parallel spots that are drawn from the same input stream but collected at different accumulation rates, i.e., at different levels of attenuation (ATN). A detailed description of the dual-spot theory of this instrument can be found in Drinovec et al. (2015). The calculation of the BC concentration from the ATN level is as follows:

$$BCc = \frac{babs(\lambda)}{\sigma abs(\lambda)} = \frac{A \times (\Delta ATN)}{Q \times \Delta t \times \sigma abs(\lambda)} \qquad (1)$$
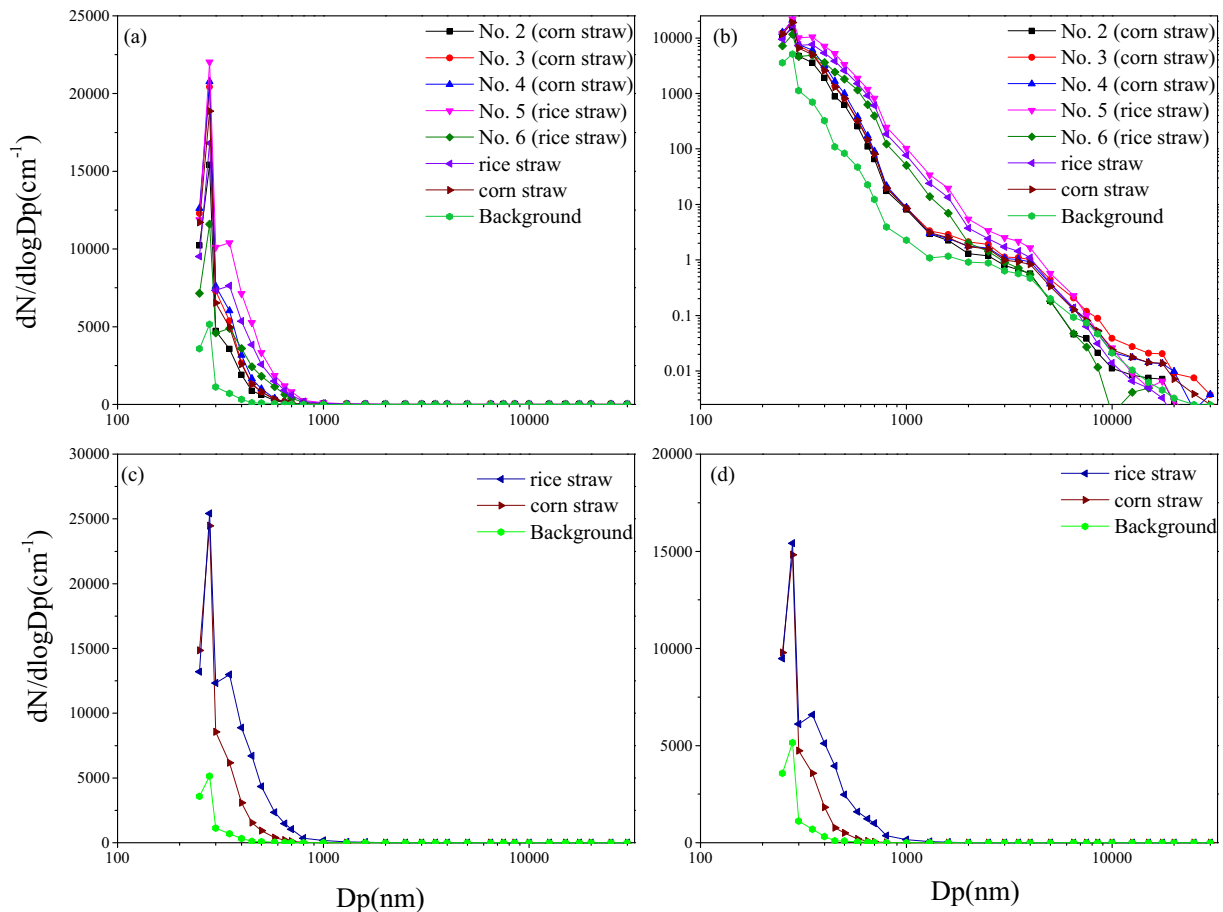
Fig. 3. Particle size distribution for different stages (phases). (a) Entire burning process (linear), (b) whole burning process (log-log), (c) flaming phase (linear), and (d) smoldering phase (linear).
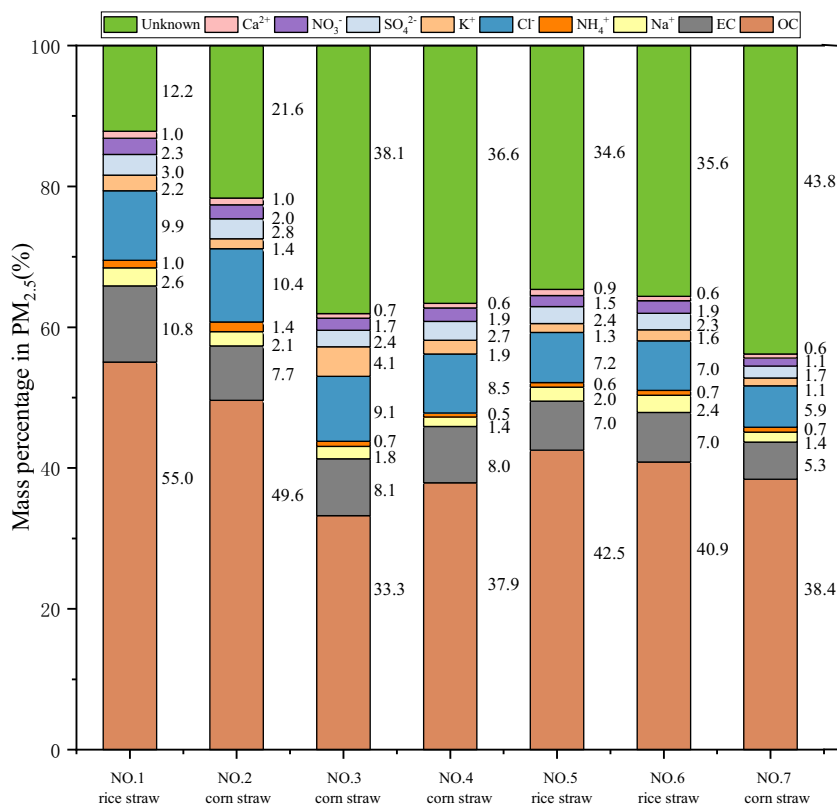
Fig. 4. Mass percentage of the major components in PM$_{2.5}$ for each experiment.

where A represents the area of the spot (which is 3 mm in diameter for the microAeth), Q is the measured flow rate, ΔATN is the change in attenuation, and Δt is the time from one measurement to the next.

We determined the aerosol absorption coefficient from the wavelength-dependent BC concentration as follows:

$$b_{abs}(\lambda) = BCc(\lambda) \times 0.001 \times \sigma(\lambda) \qquad (2)$$

where $b_{abs}(\lambda)$ is the total aerosol absorption coefficient at each wavelength (λ = 375, 470, 528, 625, and 880 nm) in units of Mm^{-1} and $BCc(\lambda)$ is the BC mass concentration (ng m^{-3}). The mass absorption cross-section (σ) values in the model MA200 aethalometer are 24.069,

19.070, 17.028, 14.091 and 10.120 m^2 g^{-1} for wavelengths of 375, 470, 528, 625 and 880 nm, respectively.

2.3. Modified combustion efficiency (MCE)

The MCE is commonly used as an indicator of the combustion conditions. The MCE is typically close to 1 during the flaming phase and ranges from 0.7 to 0.9 during the smoldering phase (Reid et al., 2005a; Yokelson et al., 1996). Ni et al. (2015) and Tian et al. (2019) both used MCE = 0.9 to differentiate between flaming and smoldering phase combustion of simulated agricultural straw burning in a combustion chamber. In this study, we suggested that a MCE higher than 0.9 represents the dominance of the flaming phase. The equation of the MCE was

Table 3
Reconstructed mass fraction of the major components to PM$_{2.5}$ mass from this study compared to similar measurements reported elsewhere (wt% of PM$_{2.5}$ mass).

Type of fuel	Measurement approach	OM	EC	Na$^+$	NH$_4^+$	K$^+$	Ca^{2+}	Cl$^-$	NO$_3^-$	SO$_4^{2-}$	References
Rice straw (n = 3)	Field	64.6 (10.8)[a]	8.3 (2.2)	2.3 (0.3)	0.8 (0.2)	1.7 (0.5)	0.8 (0.2)	8.0 (1.6)	1.9 (0.4)	2.6 (0.3)	This study
Corn straw (n = 4)	Field	55.7 (9.7)	7.3 (1.3)	1.6 (0.3)	0.8 (0.8)	2.2 (1.4)	0.7 (0.2)	8.5 (1.9)	1.7 (0.4)	2.4 (0.5)	This study
Composite profile[b] (n = 7)	Field	59.5 (10.4)	7.7 (1.7)	1.9 (0.5)	0.8 (0.3)	2.0 (1.1)	0.8 (0.2)	8.3 (1.7)	1.8 (0.4)	2.5 (0.4)	This study
Wheat straw	Field	50.1 (20.8)	7.7 (4.0)	ND[c]	3.7 (3.3)	9.9 (11.8)	ND	13.8 (14.6)	0.2 (0.2)	1.5 (1.3)	Li et al., 2007
Maize stover	Field	51.4 (17.9)	3.0 (0.7)	ND	10.0 (2.3)	8.5 (4.8)	ND	23.0 (7.1)	0.6 (0.2)	1.9 (1.1)	Li et al., 2007
Corn straw	Chamber	59.5 (18.1)	9.6 (0.9)	0.2 (0.1)	0.3 (0.02)	4.2 (0.1)	0.2 (0.1)	2.8 (0.2)	0.02 (0.01)	0.6 (0.1)	Sun et al., 2019b
Wheat straw	Chamber	63.2 (12.8)	8.8 (2.7)	0.5 (0.1)	0.6 (0.1)	5.2 (0.8)	0.2 (0.1)	4.6 (0.2)	0.2 (0.03)	0.7 (0.1)	Sun et al., 2019b
Wheat straw	Chamber	68.3 (15.0)	2.6 (2.0)	1.0 (0.8)	1.7 (0.9)	5.5 (3.9)	0.8 (0.7)	12.9 (6.3)	0.2 (0.1)	1.2 (0.5)	Ni et al., 2017
Rice straw	Chamber	61.1 (6.4)	3.2 (1.1)	2.6 (1.3)	2.5 (1.4)	10.1 (3.6)	1.2 (0.5)	21.2 (7.3)	0.5 (0.4)	3.1 (0.8)	Ni et al., 2017
Corn stalk	Chamber	98.9 (13.3)	2.5 (0.7)	1.3 (0.9)	1.3 (1.5)	2.9 (2.1)	0.9 (0.6)	8.4 (6.4)	0.2 (0.1)	2.2 (0.1)	Ni et al., 2017
Wheat straw	Chamber	31.3	11.0	ND	1.8 (0.2)	24.6 (0.4)	ND	24.2 (0.7)	0.3 (0.01)	5.4 (0.7)	Hays et al., 2005
Rice straw	Chamber	82.8	1.3	ND	ND	0.6 (0.1)	ND	1.7 (0.01)	ND	0.5 (0.01)	Hays et al., 2005

[a] The values in ( ) are the standard deviations.
[b] Average and standard deviations of each profile.
[c] ND denotes not detected or lower than the background level.

established by Ward and Radke (1993).

$$MCE = \frac{1}{1 + (ER_{CO/CO2})} \quad (3)$$

where ER_{CO/CO_2} is the excess molar mixing ratio of CO to CO_2, i.e. $\Delta CO_2 / \Delta CO$.

2.4. Chemical component statistical analysis

A one-way analysis of variance (ANOVA) with Student's t-test was used to estimate the statistical significance of differences of chimerical fraction among the source profiles. If $P > 0.05$, then there is more than a 95% probability that the two profiles are not significantly different. The statistical analyses were conducted using statistical product and service solutions (SPSS) software (Version 23 for Windows).
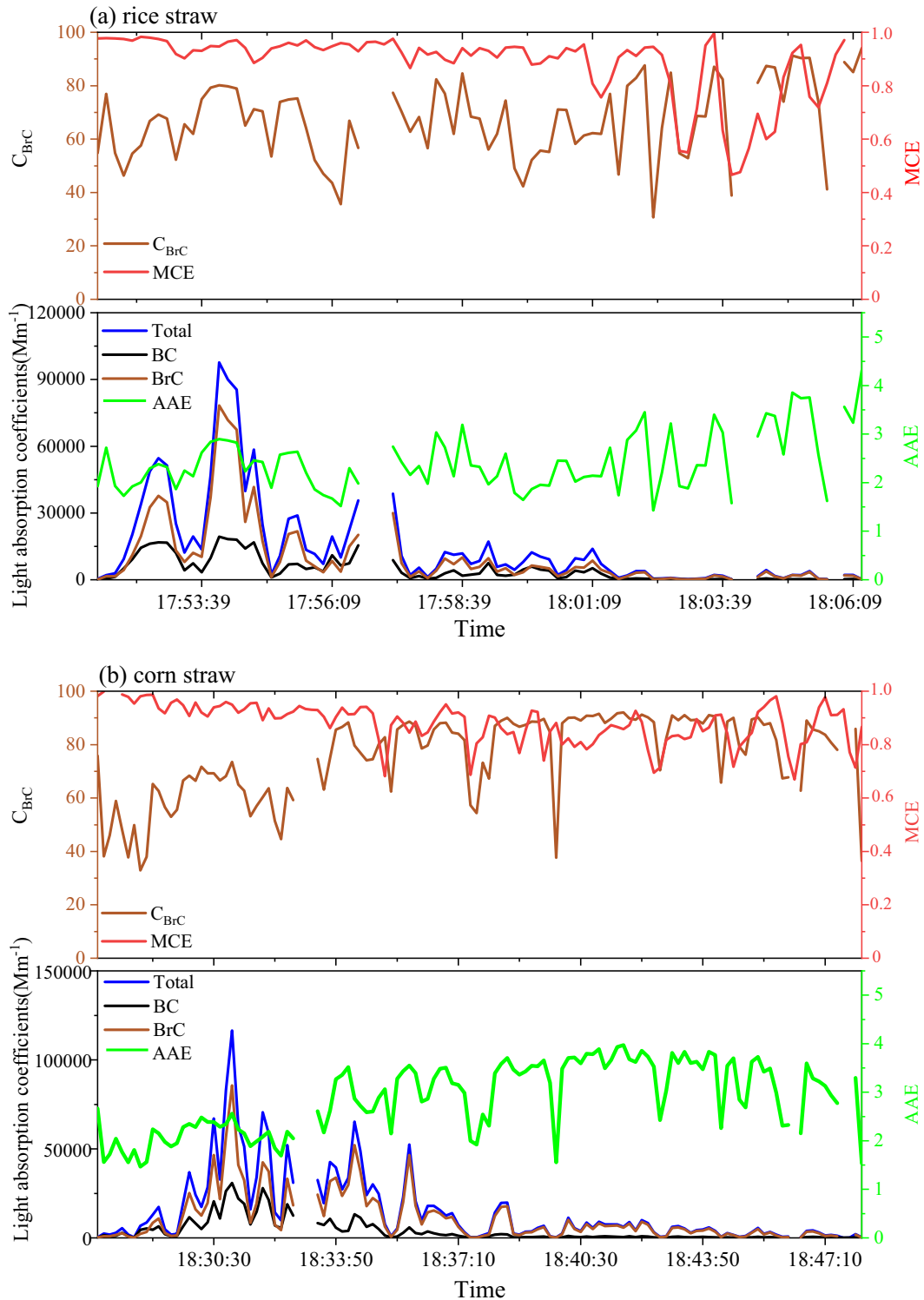

Fig. 5. Time series of the MCE, light absorption level of BrC to the total light absorption (C_{BrC}), total absorption at 375 nm, light absorption coefficients of BrC and BC at 375 nm and absorption Ångström exponent (AAE) during the burning of (a) rice straw (Fire No. 6) and (b) corn straw (Fire No. 7).

2.5. Calculation of the absorption Ångström exponent (AAE) and absorption coefficient of BrC

The wavelength (λ) dependence of particle light absorption has often been described assuming a power law as follows (Andreae and Gelencsér, 2006; Hecobian et al., 2010): $b_{abs} \sim \lambda^{-AAE}$. The AAE was calculated with wavelength pairs of 375 and 880 nm as follows:

$$AAE = -\frac{\ln\left(\frac{b_{abs}(\lambda 1)}{b_{abs}(\lambda 2))}\right)}{\ln\left(\frac{\lambda 1}{\lambda 2}\right)} \quad (4)$$

In practice, the AAE can vary depending on the selection of wavelength ranges (Moosmüller et al., 2011). In this study, λ_1 and λ_2 represent 880 and 375 nm, respectively, and $b_{abs}(\lambda_1)$ and $b_{abs}(\lambda_2)$ indicate the carbonaceous aerosol absorption coefficients at 880 and 375 nm, respectively.

Previous studies reported that pure BC absorption varies slightly from short wavelengths to long wavelengths, assuming that AAE of pure BC (AAE_{BC}) is 1 (Bergstrom et al., 2002; Bond and Bergstrom, 2006; Tian et al., 2019; Xie et al., 2019). We propose that BC is the only absorbent at the 880 nm wavelength because BC absorbs solar radiation efficiently toward the near-IR range (Bond et al., 2013; Zhu et al., 2015). The absorption coefficient of BC at a wavelength of λ nm is calculated using a fitted power law relationship at five wavelengths (Ran et al., 2016) (Eq. (5)). Thus, the absorption coefficient of BrC can be derived using Eq. (6) at each wavelength:

$$b_{abs}, BC(\lambda) = b_{abs}(880\ nm)\left(\frac{\lambda}{880}\right)^{-AAE_{BC}} \quad (5)$$

$$b_{abs,BrC}(\lambda) = b_{abs}(\lambda) - b_{abs,BC}(\lambda) \quad (6)$$

where $b_{abs,BC}(\lambda)$ and $b_{abs,BrC}(\lambda)$ are the absorption coefficients of BC and BrC, respectively, at every wavelength (λ).

3. Results and discussion

3.1. Size distribution of particle number concentration

Identifying the factors that determine the evolution of particle number distribution from biomass burning is difficult due to the large variability in fuel composition, fuel humidity, fuel bed arrangement and turbulent combustion nature. Therefore, most previous studies reported either time-integrated results or snapshots of transient phenomena. To understand the evolution of particle size distribution, it is instructive to examine the evolution of particle size distribution during the burning from the initial ignition until extinction. Based on laboratory combustion experiments, Chakrabarty et al. (2010) observed that the particle size distributions are cabined with a single diameter peak at 70 nm for wood and grass. However, Hosseini et al. (2010) reported that the major mode was in the range of 29 to 52 nm from laboratory-scale various fuels burning, which was attributable to dilution of the fresh smoke; furthermore, most fuels produced a unimodal distribution during flaming phase and strong bimodal distribution during smoldering phase in the ultrafine size range (<100 nm). The modes of the particle size distributions between 100–200 nm reported by Hays et al. (2005) using a small enclosure, and the larger geometric mean diameters were observed because their particles might have grown by condensation and coagulation with the enclosure (Hays et al., 2002).

In this study, because it is very inconvenient in the field due to the lack of electric power, we can only use a portable instrument to observe the particle size distribution. The range of instrument is limited from 250 nm to 32000 nm; thus, we can only analyze the size distribution for large particles. However, it is a fast-response instrument so that it can carry out an online observation. In addition, smaller particle mode was measured mainly in the laboratory, which was attributed to immediate dilution in order to prevent further coagulation and condensation (Hosseini et al., 2010). Particles larger than 100 nm were emitted from the field-scale biomass fires or in a small enclosure (Hays et al., 2005; LeCanut et al., 1996), which was because particles might have grown by condensation and coagulation in these conditions. In our experiments, smoke was collected within a range of 5–10 m from the fire source; thus, particle number concentration from 250 nm to 32000 nm can to some extend reveal the evolution of particle size distribution. Finally, what we want to emphasize is this: particle number concentrations and size distributions in this study do not include the particles with diameters < 250 nm.

As shown in Fig. 2a1 and b1, after the MCE reaches nearly one, it start to decrease because $\Delta CO_2/\Delta CO$ decreases, which indicates a process from the flaming phase to smoldering stage. The MCEs values showed a slight fluctuation due to the unstable meteorological conditions and dynamic state of straw combustion in the field. The highest particle number concentrations occurred during the flaming phase as shown in Fig. 2a2 and b2. It is important to note that the emission of particles, especially those between 250 and 1000 nm, decreased during the combustion phase from flaming to smoldering. The particle number concentration is primarily focused on fine particles (Dp ≤ 2500 nm), especially ultrafine particles (Dp ≤ 1000 nm) during the crop burning process; thus, we calculated the total particles from 250 to 1000 nm ($N_{250-1000}$) and from 1000 to 2500 nm ($N_{1000-2500}$) and the total volume concentration from 250 to 2500 nm ($V_{250-2500}$) for time series of straw combustion (Fig. 2a3 and b3). The $N_{250-1000}$ particles were significant higher than the $N_{1000-2500}$ particles during the whole combustion process. For rice and corn straw, the mean $N_{250-1000}$ was $3525.3 \pm 46.7\ cm^{-3}$ and $2139.0 \pm 398.1\ cm^{-3}$, respectively, and the mean $N_{1000-2500}$ was $9.1 \pm 4.8\ cm^{-3}$ and $0.8 \pm 0.1\ cm^{-3}$, respectively (Table 2). Generally, the particle concentrations decreased from the flaming to smoldering phase. Flaming was slight after ignition, and the $N_{250-1000}$ fraction was significantly higher than the $N_{1000-2500}$ while the $V_{250-2500}$ values were lower. The volume concentration increased obviously while the $N_{250-1000}$ fraction remained relatively stable from 16:20 to 16:24 in Fig. 2a3 and from 17:07 to 17:10 in Fig. 2b3 because much larger particles were emitted as the burning scope and intensity of the flaming fires increased. On average, particle number concentrations for the whole burning was higher by approximately 8 times between 250 and 2500 nm compared to that of background particles (Table 2).
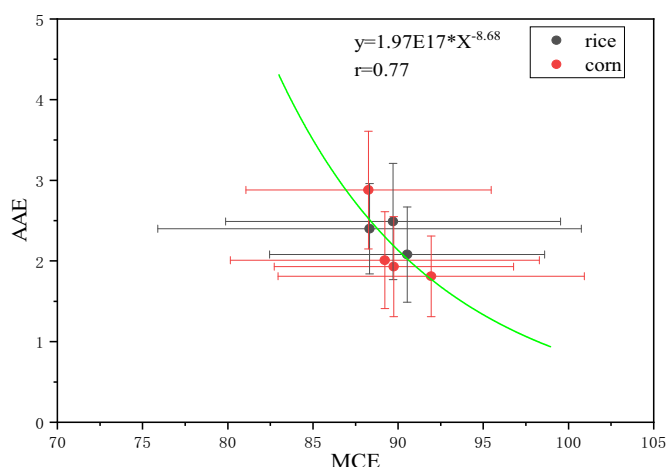

Fig. 6. Absorption Ångström exponent (AAE) at the wavelength pairs of 375 and 880 nm from burning crop residues plotted as a power function of the modified combustion efficiency (MCE). The different colors represent different biomass types as listed in the legend. (For interpretation of the references to color in this figure legend, the reader is referred to the web version of this article.)
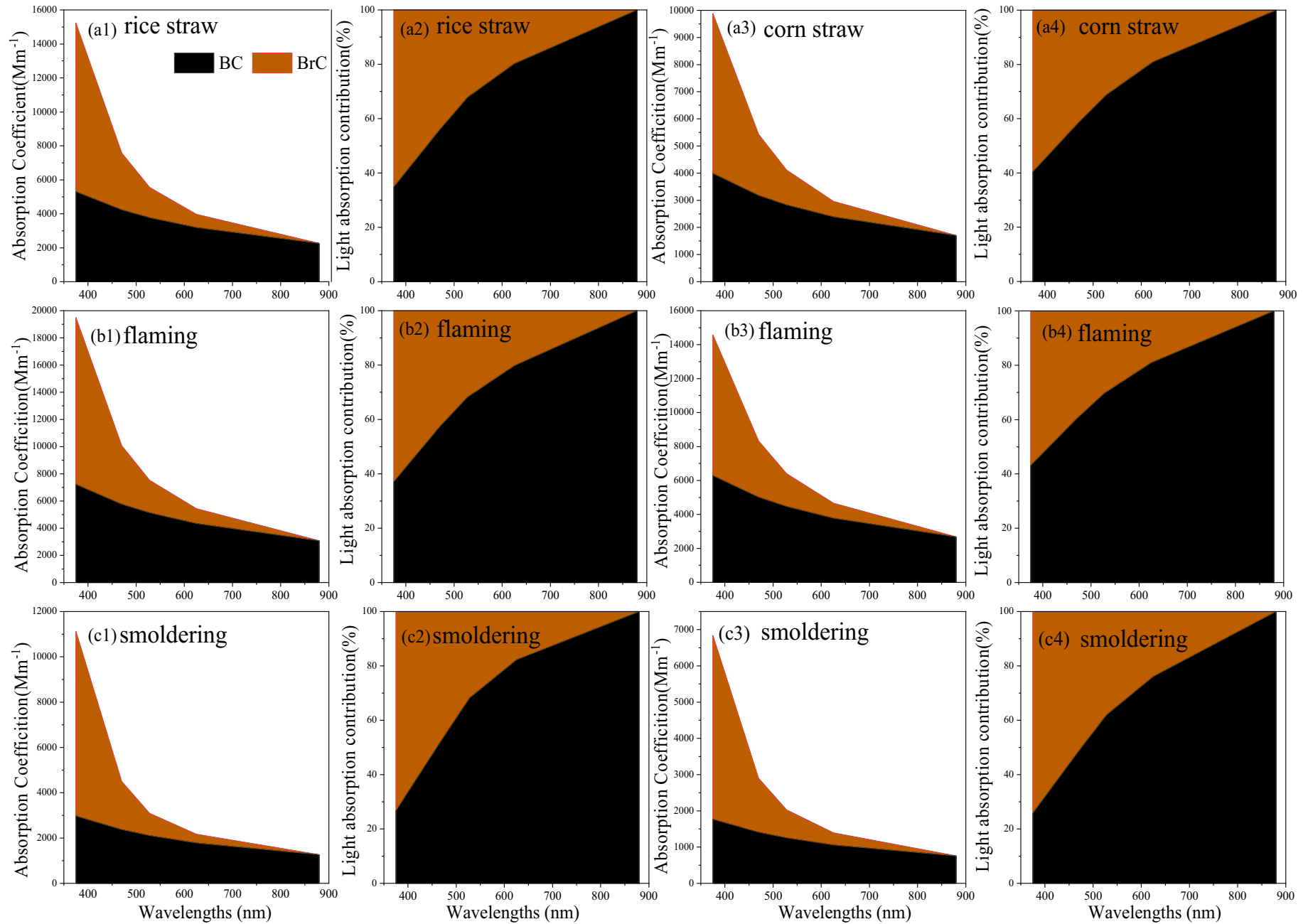
Fig. 7. Light absorption coefficients and light absorption fractions at specific wavelengths due to the BrC and BC in the total particles. (a) Whole burning process of rice (a1, a2) and corn straw (a3, a4), (b) flaming combustion phase of rice (b1, b2) and corn straw (b3, b4), (c) smoldering combustion stage of rice (c1, c2) and corn straw (c3, c4).

Mean size distributions of particles from 250 to 32000 nm for different fuels for the whole burn are shown in Fig. 3a. This was done to determine whether the concentration of particles (250 nm < Dp < 10000 nm) from biomass fires in the field was higher than the background levels of aerosols by number and by volume. The geometric mean diameter for both straw types and different combustion phases was 280 nm (Fig. 3). This is influenced by the limitation of the measuring range of OPC. Fig. 3a & b illustrate that the number concentrations of particles at background level was lower than that from residual burning in sizes between 250 and 2500 nm, because straw burning mainly emitted fine particles. Compared with the background concentration, more coarse particles for some burning processes were caused by dust associated with the soil surface. For different burning phases, most particles were emitted during the flaming process, and the number concentration was approximately 2 times higher than that from the smoldering process (Fig. 3c & d). It is worth noting that all analysis in our study is time-based not crop fuel mass-based. Analysis of fuel mass-based results will be described in another paper.

3.2. Characteristics of the $PM_{2.5}$ chemical components from crop combustion

The mass fractions of the major $PM_{2.5}$ species of each sample are shown in Fig. 4, which does not include the ambient background levels. For all experiment burning profiles, OC was most abundant and ranged from 33.3 to 55.0% of $PM_{2.5}$ ($P > 0.05$). The EC proportion of $PM_{2.5}$ varied widely from 5.3 to 10.8%, although the difference was not significant at the 95% confidence level among all combustion experiments ($P > 0.05$) (Table S1). Cl^- was the most abundant soluble ion, and its mass proportion ranged from 5.9 to 10.4%. K^+ was the next abundant soluble ion, and it ranged from 1.1 to 4.1%. These results were relatively stable in the combustion experiments ($P > 0.05$).

The average $PM_{2.5}$ mass of each test was reconstructed, and the fraction results of major components are shown in Table 3. The organic matter (OM) concentration is often derived from the OC concentration using a multiplication factor to account for the hydrogen, oxygen, and other minor species in the OM. This factor is generally estimated as 1.2–1.6 (Countess et al., 1980; Li et al., 2007; Ni et al., 2017; Reid et al., 2005a). We applied a value of 1.4 for the OM/OC ratio of the filter sampling data. Carbonaceous aerosol, including OM and EC, was the dominant component. OM ranged from 55.7 ± 9.7% for corn straw to 64.6 ± 10.8% for rice straw; and EC ranged from 7.3 ± 1.3% for corn

straw to 8.3 ± 2.2% for rice straw. The results are consistent with those from other research (Hays et al., 2005; Li et al., 2007; Ni et al., 2017; Sun et al., 2019b) as seen in Table 3. For the water soluble species, K^+ and Cl^- are the two most abundant soluble ions from agricultural burning. The mass proportion of Cl^- was 8.0 ± 1.6% and 8.5 ± 1.9% for rice straw and corn straw, respectively, and the composite average was 8.3 ± 1.7%, within the range of 4.6% to 13.8% published in other references (Table 3). K^+ is often used as a tracer for biomass burning, and it accounted for 1.7 ± 0.5% in rice straw and 2.2 ± 1.4% in corn stalk. The averaged proportion of K^+ was 2.0 ± 1.1%, which is close to those observed by Ni et al. (2017) and Sun et al. (2019b). In Table 3, the fraction of OM, EC, K^+, Cl^- in $PM_{2.5}$ from field open burning were mostly in range from 50.1–64.6%, 3.0–8.3%, 1.7–9.9% and 8.0–23.0%, which are similar to those produced from the laboratory experiments. This chemical composition characteristic is helpful for identifying the contribution of biomass burning during haze pollution (Shen et al., 2016; Sun et al., 2019a; Zhang et al., 2014).

Diagnostic ratios of chemical components can be regard as source indicators (Cao et al., 2012). The ratio of OC/EC was used to distinguish among different crop type combustion sources (Han et al., 2016). The average OC/EC ratios for corn stalk and rice straw were 5.64 ± 1.46 and 5.66 ± 0.52, respectively, which are consistent with previous studies (Cao et al., 2008; Hays et al., 2005; Li et al., 2007) but lower than those reported by Ni et al. (2017) and Sun et al. (2019b), which may be related to the more intensive flaming phase during open burning in the field than in the combustion chamber. Srinivas and Sarin (2014) reported that the ratio of K^+/EC can be used to evaluate biomass burning contributions. The values of the K^+/EC ratios were 0.20 ± 0.02 and 0.29 ± 0.16 for rice straw and corn straw, respectively, which is within the range of various published values at 0.19–3.15 (Cao et al., 2008; Hays et al., 2005; Turn et al., 1997). We also found that the K^+/OC ratio for rice straw was 0.04 ± 0.01, whereas the value was 0.06 ± 0.05 for maize residue. Similar data were observed in the studies cited above. Higher K^+/EC and K^+/OC ratios were found in the corn stalk combustion experiments.

3.3. BC and BrC absorption photometric characteristics

3.3.1. Evolution characteristics of the AAE and absorption coefficients of BC and BrC

A number of studies have reported that the absorption due to BrC contributes greatly to UV wavelengths (Andreae and Gelencsér, 2006;
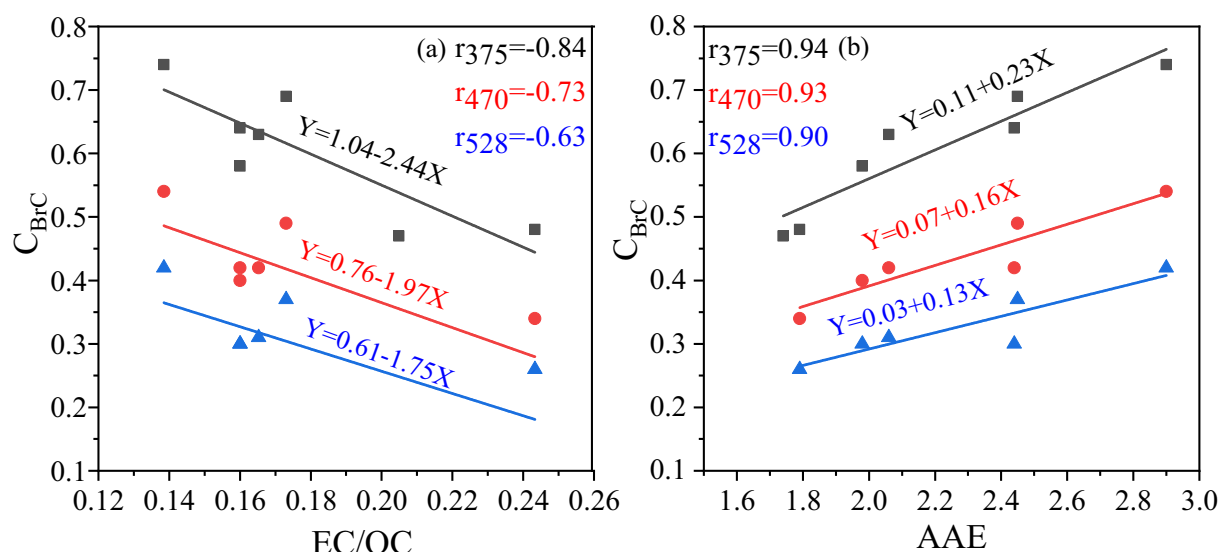

Fig. 8. Absorption contribution due to BrC vs. EC/OC and AAE (the black symbols represent 375 nm, the red symbols represent 470 nm, and the blue symbols represent 528 nm. Each point is the mean value of a test fire). (For interpretation of the references to color in this figure legend, the reader is referred to the web version of this article.)

Moosmüller et al., 2011; Schnaiter et al., 2006). The real-time MCE, AAE, absorption coefficients of BC (b_{abs-BC}) and BrC ($b_{abs-BrC}$) and contribution of BrC to the total aerosol light absorption ($C_{BrC} = b_{abs,BrC} / b_{abs}$ (λ)) at 375 nm during the complete burning cycle for fire No. 6 (rice straw) and No. 7 (corn straw) are shown in Fig. 5. The value of AAE ranges from 1.5 to 4.0 for crop straw burning. Notable differences were observed in the emission processes for the AAE, especially during smoldering. The fluctuation in C_{BrC} for rice straw burning was significantly greater than that for corn straw burning, and the maximum C_{BrC} for corn and rice straw burning reached 90% and 80%, respectively. The absorption coefficients of BC and BrC from rice straw burning at 375 nm were in the range of 17–19,326 Mm^{-1} and 88–78,314 Mm^{-1}, respectively; b_{abs-BC} and $b_{abs-BrC}$ at 375 nm ranged from 79 to 30,489 Mm^{-1} and from 97 to 46,453 Mm^{-1} for corn straw, respectively. The b_{abs-BC} and $b_{abs-BrC}$ emitted from biomass burning simultaneously increased at the ignition stage and the intermediate stage, where the flaming intensity and combustion temperature are enhanced. These two processes were both at the flaming stage and resulted in the highest b_{abs-BC} and $b_{abs-BrC}$ peaks. The smoldering stage corresponded to low b_{abs-BC} and $b_{abs-BrC}$. However, the values of C_{BrC} during the smoldering phase were higher than that during the flaming phase. Tian et al. (2019) determined that a greater proportion of light absorption by BrC occurred when different crop straw fuels were burned at a lower temperature (smoldering stages) in a combustion chamber, which was consistent with the conclusion of this experiment.

3.3.2. Characteristics of the AAE and BrC absorption

BrC absorbs radiation efficiently toward the near-UV range (Schnaiter et al., 2006), and BrC has a larger AAE in that region of the spectrum (Clarke et al., 2007). The average values of the AAE (wavelength pairs of 375 nm and 880 nm) were 2.0 ± 0.4 and 2.3 ± 0.1 for corn and rice straw, respectively, during the entire burning process. The AAEs of BrC (AAE_{BrC}) ranged from 4.5 ± 0.4 for corn straw to 5.0 ± 0.1 for rice straw (wavelength pairs of 375 nm and 625 nm). Kirchstetter and Thatcher (2012) reported that the AAE of the light-absorbing OC in wood smoke ranged from 3.0 to 7.4 with an average of 5.0. As shown in Fig. 6, the AAE exhibited a roughly negative correlation with the MCE (r = −0.77), indicating that the smoldering phases (MCE < 0.9) favored the production of BrC compared with the flaming phases (MCE ≥ 0.9). Similar negative relationships between AAE and MCE also have been reported by McMeeking et al. (2014) and Pokhrel et al. (2017) using different biomass fuels. Tian et al. (2019) indicated a negative correlation (−0.56) for agriculture residues in a chamber experiment. Generally, the relationship of AAE and MCE was indicated by the proportion of BrC and BC under different combustion conditions.

Based on Eqs. (5) and (6), b_{abs-BC} and $b_{abs-BrC}$ and the contributions of BC and BrC to the total particle light absorption at different wavelengths were calculated (Fig. 7). The light absorption coefficient of BC and BrC from different straw were presented in Table S2 at different wavelengths. The $b_{abs-BrC}$ values at 375 nm and b_{abs-BC} values at 880 nm for rice straw were both higher than those for corn straw (Table S2). As shown in Fig. 7a2 & 4, at 625 nm, 528 nm, 470 nm and 375 nm, the C_{BrC} values from corn straw burning were 19%, 31%, 41% and 60%, respectively, whereas those emitted by rice straw burning were 20%, 32%, 44% and 65%, respectively. Tian et al. (2019) reported that the BrC contributions from biomass burning experiments in a custom-made combustion chamber were as high as 68–85% at a wavelength of 370 nm. Open combustion in farmland has more oxygen and results in more efficient burning conditions compared with the simulated experiments in a chamber. Therefore, a slightly lower C_{BrC} is observed at the UV wavelength compared with that of Tian et al. (2019).

Flaming and smoldering always occurred simultaneously during the entire biomass burning process. Studies have reported that BrC was mainly emitted from biomass burning at the smoldering stage, while BC is emitted at the flaming stage (Bond et al., 2004; Chakrabarty et al., 2014). Fig. 7b & c show the BC and BrC absorption coefficients

and the fraction of light absorption at specific wavelengths by BC and BrC in the total particle light absorption profile from the burning of different crops under the flaming phase and smoldering phase. At the flaming and smoldering phase, the C_{BrC} values for rice straw were 20%, 32%, 43%, and 63% and 18%, 32%, 47%, and 73% at wavelengths of 625 nm, 528 nm, 470 nm, and 375 nm, respectively (Fig. 7b2 & 4), whereas these values for corn straw were 19%, 30%, 40%, and 57% and 24%, 38%, 51%, and 74% at wavelengths of 625 nm, 528 nm, 470 nm, and 375 nm, respectively (Fig. 7c2 & 4). During the flaming stage, the absorption coefficients of BC and BrC were higher than those during the smoldering stage, while the contributions of BrC to the total particle light absorption were lower. As the flame intensity and combustion temperature increased, the devolatilization rate increased while the volatilized organic materials would be burned rapidly (Tian et al., 2019).

Previous studies have studied the parameterization of BrC absorption based on BC/OA and EC/OC ratios and the AAE. In this study, we directly parameterize the contribution of BrC to biomass burning aerosol absorption based on the EC/OC ratio and AAE. Fig. 8 shows the percentage of absorption due to BrC at 375 nm, 470 nm and 528 nm versus EC/OC and AAE. The general pattern is that the fraction of absorption associated with BrC is the highest when the aerosol composition is dominated by OC. On the other hand, the aerosol composition dominated by EC shows a lower contribution to the total absorption from BrC at shorter wavelengths. The percentage of absorption due to BrC at 375 nm, 470 nm and 528 nm shows a reasonably good correlation with EC/OC ($r_{375} = -0.84$, $r_{470} = -0.73$, and $r_{528} = -0.63$) (Fig. 8a). We also parameterize the absorption coefficient percentage of BrC with the AAE and find that the fraction absorption due to BrC at 375 nm, 470 nm and 528 nm increases as the AAE increases ($r_{375} = 0.94$, $r_{470} = 0.93$, and $r_{528} = 0.90$) (Fig. 8b). The contribution to absorption of BrC increases as AAE increases, and a higher contribution of BrC is observed at 375 nm.

4. Conclusions

The characteristics of the particulate matter number concentration, PM$_{2.5}$ chemical components and light absorption levels of BC and BrC from field-based agricultural open burning were investigated using fast-response online and offline portable instruments in northeastern China, which has the largest area of open crop burning in China. The instruments measured evolution of particle size distribution and light absorption of BC and BrC from fire ignition to extinction to capture transient and integrated characteristics of physical and optical properties of particles from straw burning.

The results revealed that the major mode of particle size distribution for both straw types and different combustion phases was 280 nm for the range of 250 to 3200 μm; in addition, the particle number concentrations were highest during the flaming process and gradually decreased during the smoldering process based on time-based analysis. On average, particle number concentrations for the whole burning were higher by approximately 8 times between 250 and 2500 nm compared to those of background particles. Carbonaceous aerosols, including OM and EC, were the most abundant components in the PM$_{2.5}$, accounting for 59.5 ± 10.4% and 7.7 ± 1.7% respectively. Cl$^-$ and K$^+$ contributed to 8.3 ± 1.7% and 2.0 ± 1.1%, respectively. The ratios of K$^+$/OC, K$^+$/EC, and OC/EC were 0.05 ± 0.04, 0.3 ± 0.1, and 5.6 ± 1.1on the composite profiles, respectively, which is important to evaluate biomass burning contributions. The average AAE of carbonaceous aerosols was lower than AAE$_{BrC}$, and higher MCE contributed to lower AAE. On average, the fractional absorption due to BrC ranged from 65% to 20% for rice straw and 60% to 19% for corn straw from 375 nm to 625 nm, respectively; furthermore, BrC percentage was 70% at the smoldering stage and 60% at the flaming stage at 375 nm, which indicated that more BrC were emitted at smoldering stage. Generally, the fractional absorption due to BrC at different wavelengths increased as the

AAE increased and the ratio of EC/OC decreased, which can be used to parameterize biomass burning aerosol optical properties.

It is a very difficult experiment for observing field-scale biomass fires, and many instruments can't be used. Unfortunately, the particle size distribution was not measured for the ultrafine size range (<100 nm), moreover, chemical components were not observed using fast-response equipment to monitor the evolution in different combustion phases. However, our results will be substantially helpful for performing in-depth investigations of the effects of crop burning on air pollution in Northeast China. All analysis in this study is time-based not crop fuel mass-based, and we will do the latter in another paper.

Author contributions

LL Wang proposed the idea for this research. QL Wang and LL Wang mainly participated in data processing and analysis and wrote the paper. LL Wang and MM Cheng designed and conducted the experiments; and QL Wang, JD Liu, XR Li, SQ Liu, and J Chen helped finish the field experiments. XR Li and SQ Liu analyzed the aerosol chemical composition, and Q Liu provided the OPC instrument. All the authors commented and participated in the revision of the paper.

Declaration of competing interest

The authors declared that they do not have any commercial or associative interest that represents a conflict of interest in connection with the work submitted.

Acknowledgments

Appendix A. Supplementary data

Supplementary data to this article can be found online at https://doi.org/10.1016/j.scitotenv.2019.136304.

References

Alonso, B.E., Calvo, A.I., Fraile, R., Castro, A., 2012. The influence of wildfires on aerosol size distributions in rural areas. Sci. World J. 2012, 13.

Andreae, M.O., Gelencsér, A., 2006. Black carbon or brown carbon? The nature of light-absorbing carbonaceous aerosols. Atmos. Chem. Phys. 6, 3131–3148.

Bergstrom, R.W., Russell, P.B., Hignett, P., 2002. Wavelength dependence of the absorption of black carbon particles: predictions and results from the TARFOX experiment and implications for the aerosol single scattering albedo. J. Atmos. Sci. 59, 567–577.

Bond, T.C., Bergstrom, R.W., 2006. Light absorption by carbonaceous particles: an investigative review. Aerosol Sci. Technol. 40, 27–67.

Bond, T.C., Streets, D.G., Yarber, K.F., Nelson, S.M., Woo, J.H., Klimont, Z., 2004. A technology-based global inventory of black and organic carbon emissions from combustion. J. Geophys. Res.-Atmos. 109.

Bond, T.C., Doherty, S.J., Fahey, D.W., Forster, P.M., Berntsen, T., DeAngelo, B.J., Flanner, M.G., Ghan, S., Kaercher, B., Koch, D., Kinne, S., Kondo, Y., Quinn, P.K., Sarofim, M.C., Schultz, M.G., Schulz, M., Venkataraman, C., Zhang, H., Zhang, S., Bellouin, N., Guttikunda, S.K., Hopke, P.K., Jacobson, M.Z., Kaiser, J.W., Klimont, Z., Lohmann, U., Schwarz, J.P., Shindell, D., Storelvmo, T., Warren, S.G., Zender, C.S., 2013. Bounding the role of black carbon in the climate system: a scientific assessment. J. Geophys. Res.-Atmos. 118, 5380–5552.

Burkart, J., Steiner, G., Reischl, G., Moshammer, H., Neuberger, M., Hitzenberger, R., 2010. Characterizing the performance of two optical particle counters (Grimm OPC1.108 and OPC1.109) under urban aerosol conditions. J. Aerosol Sci. 41, 953–962.

Cao, G., Zhang, X., Wang, Y., Zheng, F., 2008. Estimation of emissions from field burning of crop straw in China. Chin. Sci. Bull. 53, 784–790.

Cao, J.-J., Shen, Z.-X., Chow, J.C., Watson, J.G., Lee, S.-C., Tie, X.-X., Ho, K.-F., Wang, G.-H., Han, Y.-M., 2012. Winter and summer PM2.5 chemical compositions in fourteen Chinese cities. J. Air Waste Manage. Assoc. 62, 1214–1226.

Cao, F., Zhang, S.C., Kawamura, K., Liu, X., Yang, C., Xu, Z., Fan, M., Zhang, W., Bao, M., Chang, Y., Song, W., Liu, S., Lee, X., Li, J., Zhang, G., Zhang, Y.L., 2017. Chemical characteristics of dicarboxylic acids and related organic compounds in PM2.5 during biomass-burning and non-biomass-burning seasons at a rural site of Northeast China. Environ. Pollut. 231, 654–662.

Chakrabarty, R.K., Moosmüller, H., Chen, L.W.A., Lewis, K., Arnott, W.P., Mazzoleni, C., Dubey, M.K., Wold, C.E., Hao, W.M., Kreidenweis, S.M., 2010. Brown carbon in tar balls from smoldering biomass combustion. Atmos. Chem. Phys. 10, 6363–6370.

Chakrabarty, R.K., Pervez, S., Chow, J.C., Watson, J.G., Dewangan, S., Robles, J., Tian, G., 2014. Funeral pyres in South Asia: brown carbon aerosol emissions and climate impacts. Environ. Sci. Tech. Let 1, 44–48.

Chen, J., Li, C., Ristovski, Z., Milic, A., Gu, Y., Islam, M.S., Wang, S., Hao, J., Zhang, H., He, C., Guo, H., Fu, H., Miljevic, B., Morawska, L., Thai, P., Lam, Y.F., Pereira, G., Ding, A., Huang, X., Dumka, U.C., 2017a. A review of biomass burning: emissions and impacts on air quality, health and climate in China. Sci. Total Environ. 579, 1000–1034.

Chen, W., Tong, D.Q., Dan, M., Zhang, S., Zhang, X., Pan, Y., 2017b. Typical atmospheric haze during crop harvest season in northeastern China: a case in the Changchun region. J. Environ. Sci. (China) 54, 101–113.

Cheng, Y., Engling, G., He, K.B., Duan, F.K., Ma, Y.L., Du, Z.Y., Liu, J.M., Zheng, M., Weber, R.J., 2013. Biomass burning contribution to Beijing aerosol. Atmos. Chem. Phys. 13, 7765–7781.

Clarke, A., McNaughton, C., Kapustin, V., Shinozuka, Y., Howell, S., Dibb, J., Zhou, J., Anderson, B., Brekhovskikh, V., Turner, H., Pinkerton, M., 2007. Biomass burning and pollution aerosol over North America: organic components and their influence on spectral optical properties and humidification response. J. Geophys. Res.-Atmos. 112, D12S18.

Countess, R.J., Wolff, G.T., Cadle, S.H., 1980. The Denver winter aerosol: a comprehensive chemical characterization. J. Air Pollut. Control Assoc. 30, 1194–1200.

Ding, A.J., Huang, X., Nie, W., Sun, J.N., Kerminen, V.M., Petaja, T., Su, H., Cheng, Y.F., Yang, X.Q., Wang, M.H., Chi, X.G., Wang, J.P., Virkkula, A., Guo, W.D., Yuan, J., Wang, S.Y., Zhang, R.J., Wu, Y.F., Song, Y., Zhu, T., Zilitinkevich, S., Kulmala, M., Fu, C.B., 2016a. Enhanced haze pollution by black carbon in megacities in China. Geophys. Res. Lett. 43, 2873–2879.

Ding, X., He, Q.-F., Shen, R.-Q., Yu, Q.-Q., Zhang, Y.-Q., Xin, J.-Y., Wen, T.-X., Wang, X.-M., 2016b. Spatial and seasonal variations of isoprene secondary organic aerosol in China: significant impact of biomass burning during winter. Sci. Rep-UK. 6.

Drinovec, L., Močnik, G., Zotter, P., Prévôt, A.S.H., Ruckstuhl, C., Coz, E., Rupakheti, M., Sciare, J., Müller, T., Wiedensohler, A., Hansen, A.D.A., 2015. The "dual-spot" Aethalometer: an improved measurement of aerosol black carbon with real-time loading compensation. Atmos. Meas. Tech. 8, 1965–1979.

Han, Y.M., Chen, L.-W., Huang, R.-J., Chow, J., Watson, J., Ni, H., Liu, S., Fung, K., Shen, Z., Wei, C., 2016. Carbonaceous aerosols in megacity Xi'an, China: implications of thermal/optical protocols comparison. Atmos. Environ. 132, 58–68.

Hays, M.D., Geron, C.D., Linna, K.J., Smith, N.D., Schauer, J.J., 2002. Speciation of gas-phase and fine particle emissions from burning of foliar fuels. Environ. Sci. Technol. 36, 2281–2295.

Hays, M.D., Fine, P.M., Geron, C.D., Kleeman, M.J., Gullett, B.K., 2005. Open burning of agricultural biomass: physical and chemical properties of particle-phase emissions. Atmos. Environ. 39, 6747–6764.

Hecobian, A., Zhang, X., Zheng, M., Frank, N., Edgerton, E.S., Weber, R.J., 2010. Water-soluble organic aerosol material and the light-absorption characteristics of aqueous extracts measured over the Southeastern United States. Atmos. Chem. Phys. 10, 5965–5977.

Hosseini, S., Li, Q., Cocker, D., Weise, D., Miller, A., Shrivastava, M., Miller, J.W., Mahalingam, S., Princevac, M., Jung, H., 2010. Particle size distributions from laboratory-scale biomass fires using fast response instruments. Atmos. Chem. Phys. 10, 8065–8076.

Huang, X., Ding, A., Liu, L., Liu, Q., Ding, K., Niu, X., Nie, W., Xu, Z., Chi, X., Wang, M., 2016. Effects of aerosol-radiation interaction on precipitation during biomass-burning season in East China. Atmos. Chem. Phys. 16, 10063–10082.

IPCC, 2013. Anthropogenic and natural radiative forcing. Climate Change 2013: The Physical Science Basis. Cambridge Univ. Press, New York, USA.

Islam, M.S., Saha, S.C., Sauret, E., Gu, Y., Ristovski, Z., 2015. Numerical investigation of aerosol particle transport and deposition in realistic lung airway. 6th International Conference on Computational Methods, pp. 56–68.

Ke, H., Gong, S., He, J., Zhou, C., Zhang, L., Zhou, Y., 2019. Spatial and temporal distribution of open bio-mass burning in China from 2013 to 2017. Atmos. Environ. 210, 156–165.

Kim, K.-H., Jahan, S.A., Kabir, E., Brown, R.J.C., 2013. A review of airborne polycyclic aromatic hydrocarbons (PAHs) and their human health effects. Environ. Int. 60, 71–80.

Kirchstetter, T.W., Thatcher, T.L., 2012. Contribution of organic carbon to wood smoke particulate matter absorption of solar radiation. Atmos. Chem. Phys. 12, 6067–6072.

Koppmann, R., Czapiewski, K.v., Reid, J., 2005. A review of biomass burning emissions, part I: gaseous emissions of carbon monoxide, methane, volatile organic compounds, and nitrogen containing compounds. Atmos. chem. phys. Discussions 5, 10455–10516.

LeCanut, P., Andreae, M.O., Harris, G.W., Wienhold, F.G., Zenker, T., 1996. Airborne studies of emissions from savanna fires in southern Africa. 1. Aerosol emissions measured with a laser optical particle counter. J. Geophys. Res.-Atmos. 101, 23615–23630.

Li, X., Wang, S., Duan, L., Hao, J., Li, C., Chen, Y., Yang, L., 2007. Particulate and trace gas emissions from open burning of wheat straw and corn stover in China. Environ. Sci. Technol. 41, 6052–6058.

Li, X., Wang, L., Wang, Y., Wen, T., Yang, Y., Zhao, Y., Wang, Y., 2012. Chemical composition and size distribution of airborne particulate matters in Beijing during the 2008 Olympics. Atmos. Environ. 50, 278–286.

Li, L., Qian, J., Ou, C.Q., Zhou, Y.X., Guo, C., Guo, Y., 2014. Spatial and temporal analysis of Air Pollution Index and its timescale-dependent relationship with meteorological factors in Guangzhou, China, 2001–2011. Environ. Pollut. 190, 75–81.

McMeeking, G., Fortner, E., Onasch, T., Taylor, J., Flynn, M., Coe, H., Kreidenweis, S., 2014. Impacts of nonrefractory material on light absorption by aerosols emitted from biomass burning. J. Geophys. Res.-Atmos. 119, 12,272–12,286.

Mehmood, K., Chang, S., Yu, S., Wang, L., Li, P., Li, Z., Liu, W., Rosenfeld, D., Seinfeld, J.H., 2017. Spatial and temporal distributions of air pollutant emissions from open crop straw and biomass burnings in China from 2002 to 2016. Environ. Chem. Lett. 16, 301–309.

Moosmüller, H., Chakrabarty, R.K., Ehlers, K.M., Arnott, W.P., 2011. Absorption Ångström coefficient, brown carbon, and aerosols: basic concepts, bulk matter, and spherical particles. Atmos. Chem. Phys. 11, 1217–1225.

Ni, H., Han, Y., Cao, J., Chen, L.W.A., Tian, J., Wang, X., Chow, J.C., Watson, J.G., Wang, Q., Wang, P., Li, H., Huang, R.-J., 2015. Emission characteristics of carbonaceous particles and trace gases from open burning of crop residues in China. Atmos. Environ. 123, 399–406.

Ni, H., Tian, J., Wang, X., Wang, Q., Han, Y., Cao, J., Long, X., Chen, L.-W.A., Chow, J.C., Watson, J.G., 2017. PM2. 5 emissions and source profiles from open burning of crop residues. Atmos. Environ. 169, 229–237.

Penner, J.E., Dickinson, R.E., O'Neill, C.A., 1992. Effects of aerosol from biomass burning on the global radiation budget. Science 256, 1432–1434.

Pokhrel, R.P., Beamesderfer, E.R., Wagner, N.L., Langridge, J.M., Lack, D.A., Jayarathne, T., Stone, E.A., Stockwell, C.E., Yokelson, R.J., Murphy, S.M., 2017. Relative importance of black carbon, brown carbon, and absorption enhancement from clear coatings in biomass burning emissions. Atmos. Chem. Phys. 17, 5063–5078.

Ran, L., Deng, Z.Z., Wang, P.C., Xia, X.A., 2016. Black carbon and wavelength-dependent aerosol absorption in the North China Plain based on two-year aethalometer measurements. Atmos. Environ. 142, 132–144.

Reid, J., Koppmann, R., Eck, T., Eleuterio, D., 2005a. A review of biomass burning emissions part II: intensive physical properties of biomass burning particles. Atmos. Chem. Phys. 5, 799–825.

Reid, J.S., Eck, T.F., Christopher, S.A., Koppmann, R., Dubovik, O., Eleuterio, D.P., Holben, B.N., Reid, E.A., Zhang, J., 2005b. A review of biomass burning emissions part III: intensive optical properties of biomass burning particles. Atmos. Chem. Phys. 5, 827–849.

Schnaiter, M., Gimmler, M., Llamas, I., Linke, C., Jaeger, C., Mutschke, H., 2006. Strong spectral dependence of light absorption by organic carbon particles formed by propane combustion. Atmos. Chem. Phys. 6, 2981–2990.

Shen, Z., Sun, J., Cao, J., Zhang, L., Zhang, Q., Lei, Y., Gao, J., Huang, R.-J., Liu, S., Huang, Y., Zhu, C., Xu, H., Zheng, C., Liu, P., Xue, Z., 2016. Chemical profiles of urban fugitive dust PM2.5 samples in Northern Chinese cities. Sci. Total Environ. 569, 619–626.

Srinivas, B., Sarin, M., 2014. PM2. 5, EC and OC in atmospheric outflow from the Indo-Gangetic Plain: temporal variability and aerosol organic carbon-to-organic mass conversion factor. Sci. Total Environ. 487, 196–205.

Sun, J., Shen, Z., Zhang, L., Lei, Y., Gong, X., Zhang, Q., Zhang, T., Xu, H., Cui, S., Wang, Q., Cao, J., Tao, J., Zhang, N., Zhang, R., 2019a. Chemical source profiles of urban fugitive dust PM2.5 samples from 21 cities across China. Sci. Total Environ. 649, 1045–1053.

Sun, J., Shen, Z., Zhang, Y., Zhang, Q., Lei, Y., Huang, Y., Niu, X., Xu, H., Cao, J., Ho, S.S.H., Li, X., 2019b. Characterization of PM2.5 source profiles from typical biomass burning of maize straw, wheat straw, wood branch, and their processed products (briquette and charcoal) in China. Atmos. Environ. 205, 36–45.

Tian, J., Wang, Q., Ni, H., Wang, M., Zhou, Y., Han, Y., Shen, Z., Pongpiachan, S., Zhang, N., Zhao, Z., Zhang, Q., Zhang, Y., Long, X., Cao, J., 2019. Emission characteristics of primary brown carbon absorption from biomass and coal burning: development of an optical emission inventory for China. J. Geophys. Res.-Atmos. 124, 1879–1893.

Turn, S.Q., Jenkins, B.M., Chow, J.C., Pritchett, L.C., Campbell, D., Cahill, T., Whalen, S.A., 1997. Elemental characterization of particulate matter emitted from biomass burning: wind tunnel derived source profiles for herbaceous and wood fuels. J. Geophys. Res.-Atmos. 102, 3683–3699.

Wang, J., Hu, Z., Chen, Y., Chen, Z., Xu, S., 2013. Contamination characteristics and possible sources of PM10 and PM2.5 in different functional areas of Shanghai, China. Atmos. Environ. 68, 221–229.

Wang, L., Xin, J., Li, X., Wang, Y., 2015. The variability of biomass burning and its influence on regional aerosol properties during the wheat harvest season in North China. Atmos. Res. 157, 153–163.

Wang, J., Xing, J., Mathur, R., Pleim, J.E., Wang, S., Hogrefe, C., Gan, C.-M., Wong, D.C., Hao, J., 2017. Historical trends in PM2.5-related premature mortality during 1990–2010 across the Northern Hemisphere. Environ. Health. Persp. 125, 400–408.

Ward, D., Radke, L., 1993. Emissions measurements from vegetation fires: a comparative evaluation of methods and results. Fire Environ. Ecol. Atmos. Clim. Imp. Veg. Fires. 13, 53–76.

Xie, C., Xu, W., Wang, J., Wang, Q., Liu, D., Tang, G., Chen, P., Du, W., Zhao, J., Zhang, Y., Zhou, W., Han, T., Bian, Q., Li, J., Fu, P., Wang, Z., Ge, X., Allan, J., Coe, H., Sun, Y., 2019. Vertical characterization of aerosol optical properties and brown carbon in winter in urban Beijing. China. Atmos. Chem. Phys. 19, 165–179.

Yan, X., Ohara, T., Akimoto, H., 2006. Bottom-up estimate of biomass burning in mainland China. Atmos. Environ. 40, 5262–5273.

Yokelson, R.J., Griffith, D.W.T., Ward, D.E., 1996. Open-path Fourier transform infrared studies of large-scale laboratory biomass fires. J. Geophy. Res-Atmos. 101, 21067–21080.

Yuyun, B., Yajing, W., Chunyu, G., 2010. Straw resource quantity and its regional distribution in China. Journal of Agricultural Mechanization Research 3, 1–7.

Zhang, Q., Shen, Z., Cao, J., Ho, K., Zhang, R., Bie, Z., Chang, H., Liu, S., 2014. Chemical profiles of urban fugitive dust over Xi'an in the south margin of the Loess Plateau, China. Atmos. Pollut. Res. 5, 421–430.

Zhang, T., Wooster, M.J., Green, D.C., Main, B., 2015. New field-based agricultural biomass burning trace gas, PM 2.5, and black carbon emission ratios and factors measured in situ at crop residue fires in Eastern China. Atmos. Environ. 121, 22–34.

Zhang, L., Liu, Y., Hao, L., 2016. Contributions of open crop straw burning emissions to PM2.5 concentrations in China. Environ. Res. Lett. 11, 014014.

Zhu, C.-S., Cao, J.-J., Ho, K.-F., Chen, L.W.A., Huang, R.-J., Wang, Y.-C., Li, H., Shen, Z.-X., Chow, J.C., Watson, J.G., Su, X., Wang, Q., Xiao, S., 2015. The optical properties of urban aerosol in northern China: a case study at Xi'an. Atmos. Res. 160, 59–67.

Zhuang, Y., Li, R., Yang, H., Chen, D., Chen, Z., Gao, B., He, B., 2018. Understanding temporal and spatial distribution of crop residue burning in China from 2003 to 2017 using MODIS data. Remote Sens. 10, 390.